RSC Advances

PAPER

View Article Online
View Journal | View Issue

Cite this: *RSC Adv.*, 2018, **8**, 22226

Facile synthesis of partially oxidized Mn_3O_4-functionalized carbon cathodes for rechargeable Li–O_2 batteries†

Juhyoung Kim, Inhan Kang, Soyeon Kim and Jungwon Kang *

Received 5th April 2018
Accepted 7th June 2018

DOI: 10.1039/c8ra02920b

rsc.li/rsc-advances

High charging overpotential (low energy efficiency) is one of the most important challenges preventing the use of current nonaqueous Li–O_2 batteries. This study demonstrates direct *in situ*-incorporation of metal oxides on carbon during synthesis and the associated application to nonaqueous Li–O_2 battery catalysts. The partially oxidized Mn_3O_4 (Mn_3O_4/Mn_5O_8)-incorporating carbon cathode shows an average overpotential reduction of ~8% charge/discharge during 40 cycles in a rechargeable nonaqueous Li–O_2 cell. Here, we suggested the possibility that only a small amount of the oxide species (<5%) could show catalytic effects during charge in a rechargeable Li–O_2 cell.

Introduction

Lithium–oxygen (Li–O_2) batteries have attracted considerable scientific attention due to their high theoretical specific energy density (~3 kW h kg^{-1}), which could possibly satisfy the demand for use in improved electric vehicles, if realised.[1–4] However, despite this high energy density, Li–O_2 batteries present many scientific challenges that have also prevented their commercialization, such as their large polarization, low round-trip efficiency and poor cyclability.[5–7] Typically, a reachargeable nonaqueous Li–O_2 battery is composed of a Li metal anode, a nonaqueous Li^+ ion conducting electrolyte and a porous cathode and is based on a net electrochemical reaction ($2Li^+ + O_2 + 2e^- \leftrightarrow Li_2O_2$) with a thermodynamically determined reversible potential (U_0 = 2.96 V, *versus* Li/Li^+).[8–10] However, there are large differences between the theoretical and empirical potential, and this problem presents one of the greatest challenges. Early studies on Li–O_2 batteries showed a modest overpotential (~0.3 V) for discharging but a high overpotential (~1.5 V),[11,12] and the charge overpotential is particularly large due to decomposition of the insulating discharge product, Li_2O_2.[13] This overpotential results in a reduction in energy efficiency (the energy released during discharging/the energy required during charging).

Many efforts have been made to suppress this energy loss during either the discharge or recharge process by adding a catalytic substance, such as a metal and a metal oxide into the carbon.[14] However, owing to the catalytic effects of certain materials, the use of precious metals (Pt, Au, Ru *etc.*) and the complex routes used to synthesize metal oxides are undesirable.[15,16] In addition, when only mechanical mixing of catalysts containing carbon is employed,[17] electronic conductivity of the cathodes and inappropriate contact between the catalyst/carbon interfaces results. Furthermore, the metal/carbon ratio needs to be carefully controlled for heavy metals during the mixing process, as it can cause a decrease in the gravimetric energy density.[18,19]

This study demonstrates the direct *in situ*-incorporation of metal oxides on carbon during synthesis and the associated application to nonaqueous Li–O_2 battery catalysts. The partially oxidized Mn_3O_4 (Mn_3O_4/Mn_5O_8)-incorporated carbon cathode shows an average reduction of ~8% charge/discharge overpotential during 40 cycles in a rechargeable nonaqueous Li–O_2 cell.

Experimental

Preparation of materials

The detailed preparation procedure for partially oxidized Mn_3O_4 (Mn_3O_4/Mn_5O_8)-incorporated carbon is shown in Scheme 1. Manganese(II) acetate tetrahydrate ($(CH_3COO)_2$-$Mn \cdot 4H_2O$-98%, Daejung) was dissolved in ethanol (99.9%, Daejung). Carbon paper (P50, AvCarb®) was dipped in the manganese acetate solution and then dried, and the manganese acetate-immersed P50 was heated at 300 °C in air for 10 h. Manganese oxide-functionalized P50 was obtained, and the manganese oxide was determined as being partially oxidized Mn_3O_4 (Mn_3O_4/Mn_5O_8)-functionalized carbon using X-ray photoelectron spectroscopy (XPS), transmission electron microscope (TEM), and X-ray diffraction (XRD) patterns.

TEGDME (tetraethylene glycol dimethyl ether, ≥99%) was purchased from Sigma-Aldrich and dried over a freshly activated molecular sieve with a 4 Å pore size. LiTFSI (bis(trifluoromethane)sulfonimide lithium salt, Sigma-Aldrich) was dried in a vacuum oven at 150 °C for 24 h. P50 carbon paper was

Department of Advanced Materials Science and Engineering, Mokpo National University, 61 dorim-ri, 1666 Yeongsan-ro, Cheonggye-myeon, Muan-gun, Jeonnam, South Korea. E-mail: jwkang17@mokpo.ac.kr

† Electronic supplementary information (ESI) available. See DOI: 10.1039/c8ra02920b

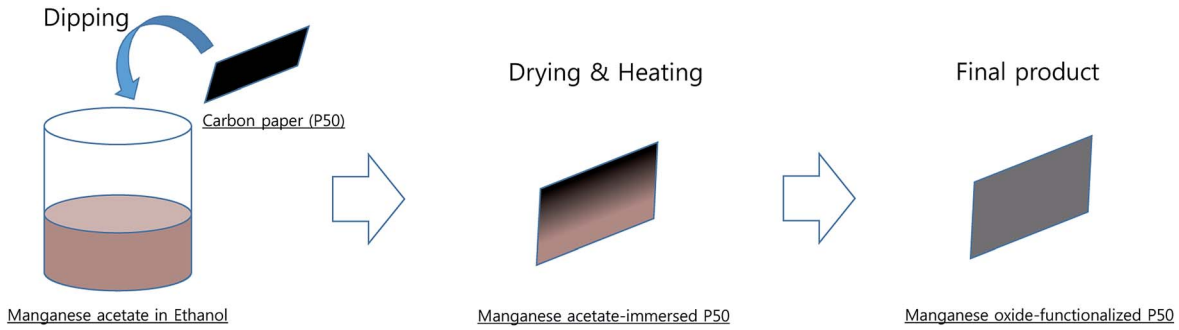

Scheme 1 Partially oxidized Mn_3O_4 (Mn_3O_4/Mn_5O_8)-incorporated carbon preparation procedure.

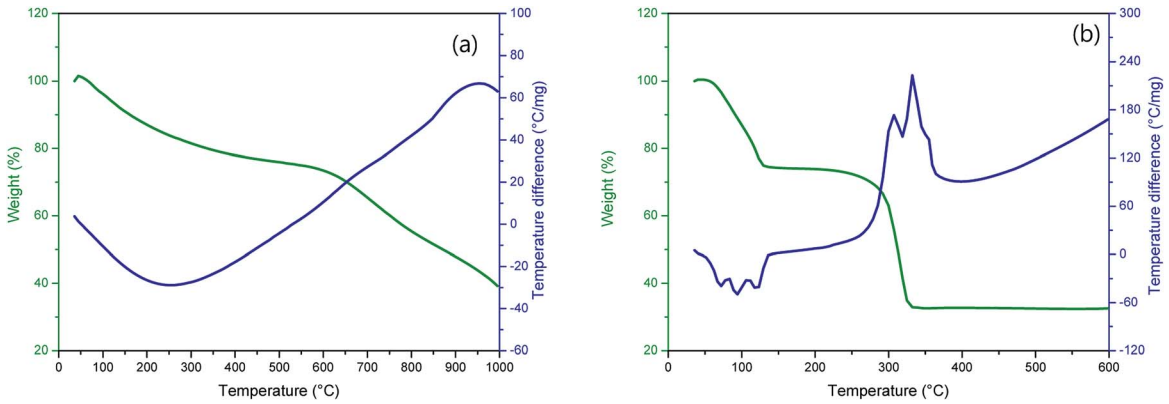

Fig. 1 TG-DTA curves of (a) P50 in nitrogen, and (b) manganese(II) acetate tetrahydrate in air.

purchased from AvCarb®. Carbon cathodes were dried in a vacuum oven (150 °C) and transferred to an Ar-filled glove box for cell fabrication.

Characterization of materials

Morphology and elemental mapping were conducted using field-emission transmission electron microscopy (FETEM) (Philips Tecnai F20) at 200 kV; XPS analysis was conducted using Al Kα as the X-ray source (Thermo VG Scientific instrument, Multilab 2000); the powder X-ray diffraction pattern (XRD) of prepared samples was measured using a PANalytical X'Pert PRO Multi-Purpose X-ray Diffractometer; and thermal analysis was conducted using a Mettler Toledo. X-ray absorption spectroscopy (XAS) was performed using a Rigaku Model R-XAS.

Fabrication of Li–O_2 cells

Swagelok-type cells were composed of a Li metal anode (Honjo Metal Co.) with carbon (AvCarb P50) as the prepared cathode and the GF (GF/C™, Whatman™) as a separator and the cell fabricated in an Ar-filled glove box (MBraun, H_2O < 1 ppm). High purity oxygen gas (>99.999%) was blown into the carbon cathode through a capillary (inlet) attached to the upper side of the Swagelok®-type cells and then out of the cathode through another capillary (outlet), to replace argon with oxygen within the cell. An oxygen environment of ~1.5 bar was maintained during discharging and charging by opening the inlet capillary and closing the outlet. Electrochemical properties for the assembled Li–O_2 cells were analysed using a VMP3 potentiostat (Biologic Science Instrument).

Results and discussion

Fig. 1 shows TG-DTA curves of (a) P50 in nitrogen and (b) manganese(II) acetate tetrahydrate in air. The TG curve (Fig. 1a, green) of P50 shows a weight loss of ~30% at ~600 °C, and the corresponding endothermic peak is shown in the DTA curve (Fig. 1a, blue). This weight loss implies the occurrence of

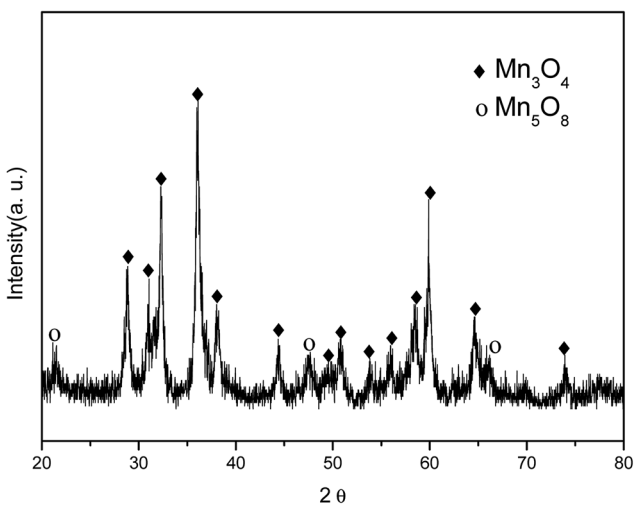

Fig. 2 XRD pattern of Mn-acetate heated at 300 °C for 10 h in air.

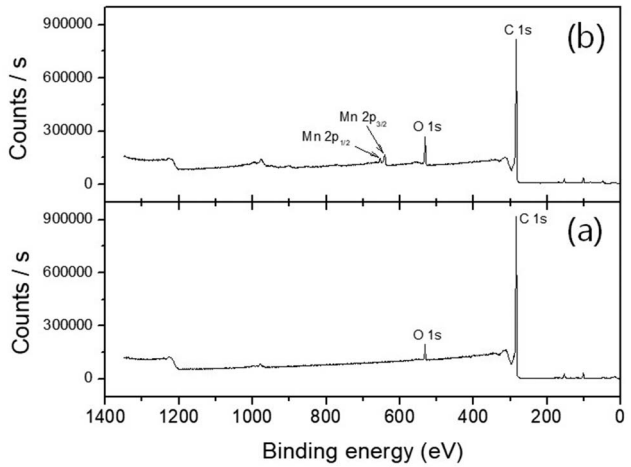

Fig. 3 XPS survey scan analysis of (a) pristine P50 and (b) partially oxidized Mn_3O_4-functionalized P50.

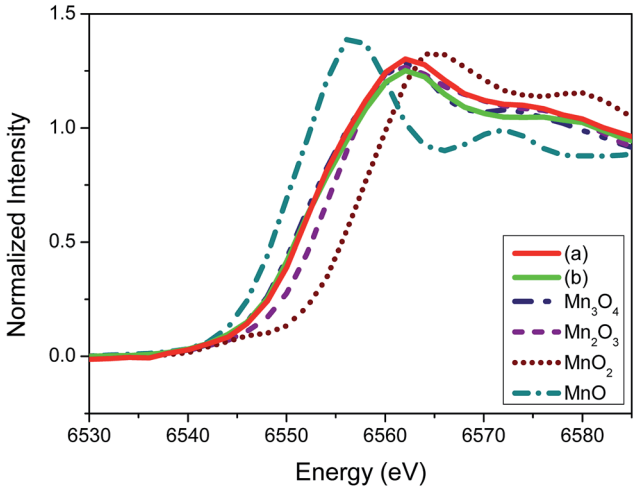

Fig. 5 XANES spectra of (a) the partially oxidized Mn_3O_4-functionalized P50, (b) the powder of Mn-acetate heated at 300 °C for 10 h in air and, the references corresponding to Mn_3O_4, Mn_2O_3, MnO_2 and MnO.

moisture desorption, thermal desorption of organic and inorganic matter absorbed by activated carbon, and oxidation of amorphous carbon.[20] In the TG-DTA curves shown in Fig. 1b, it is evident that manganese(II) acetate tetrahydrate begins to lose water at around room temperature to produce anhydrous salts that are then decomposed to MnO at about 320 °C.[21] To conduct a thermal analysis, an annealing temperature of 300 °C was used for the direct *in situ*-incorporation of manganese oxides on carbon during synthesis, as carbon paper (P50) is drastically oxidized at temperatures over 400 °C. Fragments of partially oxidized P50 were observable in the sample heated at 400 °C; this sample showed poor electrochemical properties, as evidenced in Fig. S1 (in the ESI†).

The incorporation of manganese oxide to carbon in the final product was confirmed by X-ray diffraction (XRD); however, it was not possible to obtain a distinct diffraction pattern of manganese oxide, as shown in Fig. S2 (in the ESI†), as the manganese-oxide included only a few amount (4.33 w%, element analysis by TEM). Fig. 2 shows the XRD pattern of Mn-acetate when heated only to 300 °C; the powder is verified as a composite of major-Mn_3O_4/minor-Mn_5O_8. Based on this result, it was hypothesized that the final product of partially oxidized Mn_3O_4 (Mn_3O_4/Mn_5O_8)-incorporated carbon could be obtained (as shown in Scheme 1).

The precise stoichiometry of the manganese oxide-incorporated carbon obtained was then further investigated using XPS. Fig. 3 shows XPS survey scan analysis at a binding energy range between 0 and 1400 eV, where there is no evidence of Mn-related signals in the pristine P50 (Fig. 3a). However, the manganese oxide-functionalized P50 clearly shows doublet splitting of Mn $2p_{3/2}$ and Mn $2p_{1/2}$ at binding energies of 642.18 eV and 654.21 eV, respectively, as shown in Fig. 3b.[22] Various Mn ionic species exist in the sample of partially oxidized manganese oxide-incorporated carbon, and the position and intensity of the XPS peaks are considered to identify a consistent oxide formula.

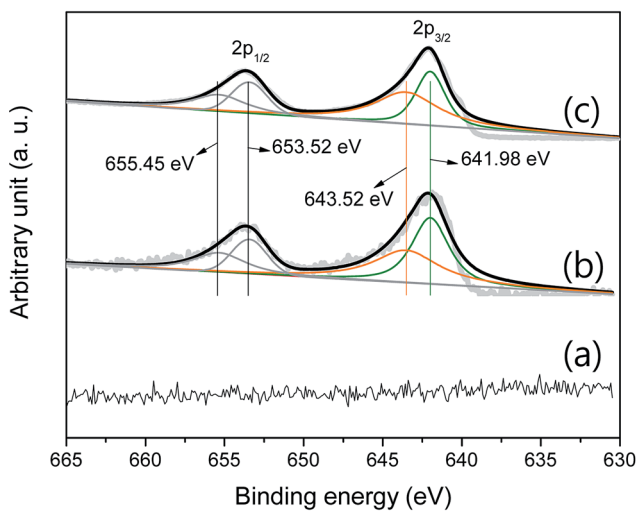

Fig. 4 Curve-fitted XPS Mn 2p of (a) pristine P50, (b) partially oxidized Mn_3O_4-functionalized P50, and (c) powder of Mn-acetate heated at 300 °C for 10 h in air.

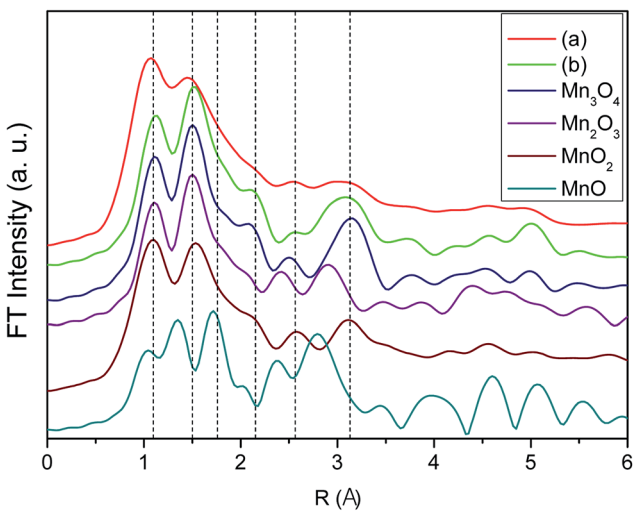

Fig. 6 XANES spectra of (a) the partially oxidized Mn_3O_4-functionalized P50, (b) the powder of Mn-acetate heated at 300 °C for 10 h in air and, the references corresponding to Mn_3O_4, Mn_2O_3, MnO_2 and MnO.

Fig. 4 shows the curve-fitted XPS Mn 2p. There is no signal that indicates a series of manganese oxides in the pristine P50 sample (Fig. 4a). Fig. 4b shows the curve-fitted Mn 2p of the partially oxidized Mn_3O_4-functionalized P50, which was prepared as illustrated in Scheme 1 (with a heating temperature of 300 °C). Fig. 4c shows results of Mn-acetate powder heated at 300 °C for 10 h in air, which was examined by XRD and determined as a composite of major-Mn_3O_4/minor-Mn_5O_8. XRD did not confirm the presence of manganese oxide in the sample of the partially oxidized Mn_3O_4-functionalized P50, due to the low amount of manganese oxide present. However, the XPS signal was analogous in samples of the partially oxidized Mn_3O_4-functionalized P50 (Fig. 4b) and the powder of Mn-acetate heated at 300 °C for 10 h in air (Fig. 4c). The oxidation states of the Mn atom in manganese oxides were then further examined by peak deconvolution, on the assumption that the intensity ratios related to Mn^{2+} and Mn^{4+} have corresponding peak positions of 641.98 and 643.52 eV, respectively.

Based on the similarity of the XPS signal for both samples (Fig. 4b and c), it was considered that the species of functionalized manganese oxides were a composite of major-Mn_3O_4/minor-Mn_5O_8; this was confirmed by XRD analysis.

To elucidate further on the oxidation state of the manganese oxide-incorporated carbon obtained, X-ray absorption near-edge structure (XANES) analysis was conducted. Fig. 5 shows XANES spectra of the partially oxidized Mn_3O_4-functionalized P50 (a), the powder of Mn-acetate heated at 300 °C for 10 h in air (b) and the references corresponding to Mn_3O_4, Mn_2O_3, MnO_2 and MnO. The observed Mn valence in the partially oxidized Mn_3O_4-functionalized P50 (Fig. 5a) and the powder of Mn-acetate heated at 300 °C for 10 h in air (Fig. 5b) shows similarity, and the XANES spectra of both samples are analogous to the Mn_3O_4 reference (Fig. 5). The XANES spectra of Mn_2O_3 (Mn^{+3} state) shows slightly higher state than the partially oxidized Mn_3O_4-functionalized P50 of which oxidation state is clearly less than Mn^{+4} (MnO_2), but greater than Mn^{+2} (MnO) as depicted in Fig. 4. This trend is clearly in accordance with the XPS characterization.

The extended X-ray absorption fine structure (EXAFS) spectra of the partially oxidized Mn_3O_4-functionalized P50 (Fig. 6) provide

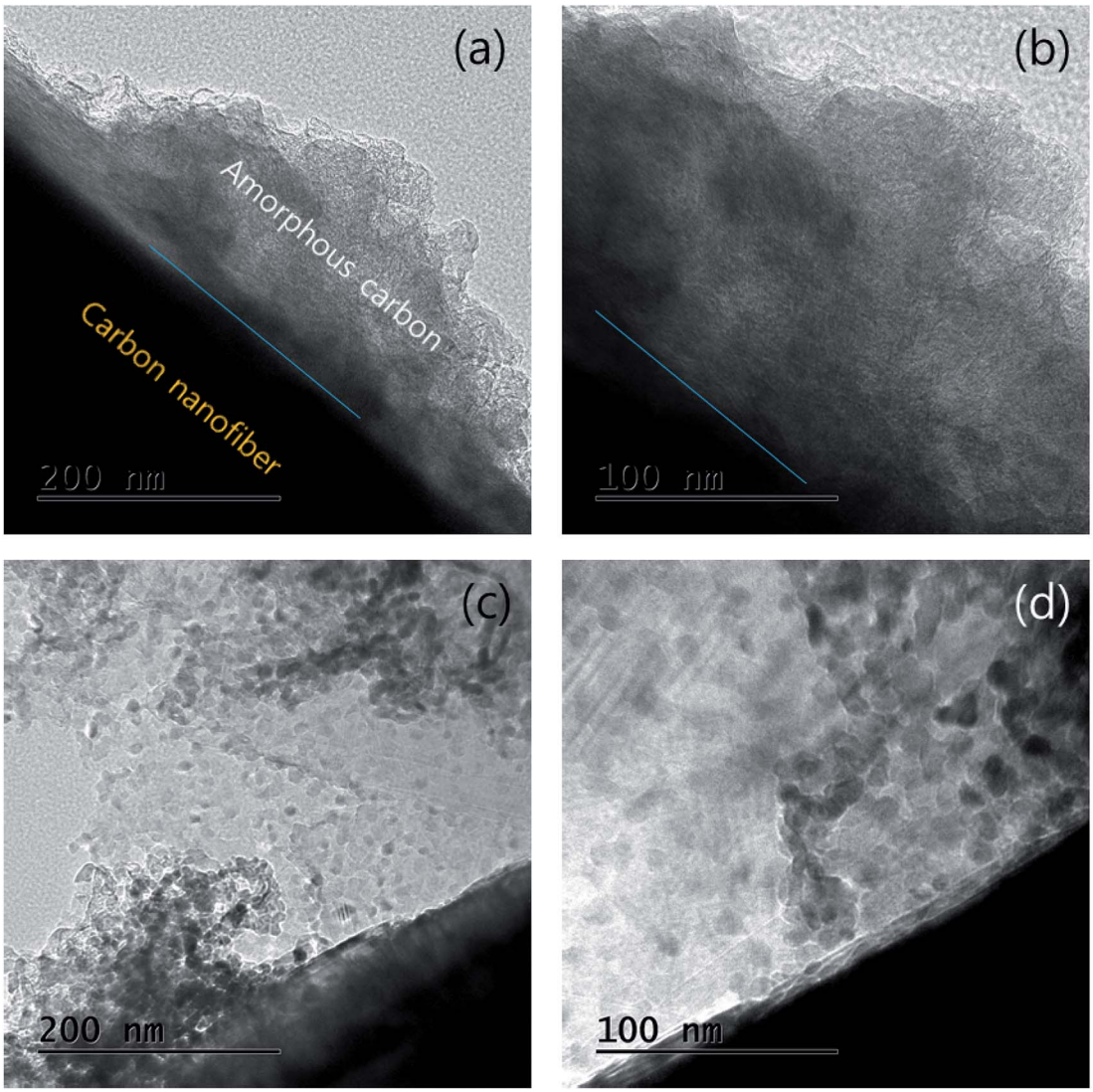

Fig. 7 HR-TEM images of (a and b) pristine P50 and (c and d) partially oxidized Mn_3O_4-functionalized P50.

further information about the related phases. Fig. 6 shows the EXAFS spectra of the partially oxidized Mn_3O_4-functionalized P50 (a), the powder of Mn-acetate heated at 300 °C for 10 h in air (b) and the references corresponding to Mn_3O_4, Mn_2O_3, MnO_2 and MnO. The EXAFS results are also in the similar context for defining our prepared sample as the partially oxidized Mn_3O_4-functionalized P50. The EXAFS spectra of the partially oxidized Mn_3O_4-functionalized P50 (Fig. 6a) is analogous to the sample of Mn-acetate heated at 300 °C for 10 h in air (Fig. 6b) of which feature well matches that of Mn_3O_4 (Fig. 6). Unfortunately the detailed local environment of Mn in the partially oxidized Mn_3O_4-functionalized P50 cannot be easily investigated by EXAFS due to its little amount of manganese oxide contents. This XANES and EXAFS results clearly follow the trend observed with XPS and XRD characterization in which our prepared sample in the procedure (Scheme 1) defined the partially oxidized Mn_3O_4-functionalized P50.

The particles and shape of partially oxidized Mn_3O_4-functionalized P50 were confirmed using HR-TEM. Fig. 7 shows HR-TEM images of (a and b) pristine P50 and (c and d) partially oxidized Mn_3O_4-functionalized P50. The absence of particles is evident, and only amorphous carbon exists on the carbon nanofiber in the pristine P50 sample (Fig. 5a and b). However, Fig. 7c and d show that the nanoparticles of manganese oxides are well dispersed in amorphous carbon in the partially oxidized Mn_3O_4-functionalized P50. The solid contact formed during the *in situ* method between carbon and oxide-particles led to catalytic effects (reduction of the overpotential), despite the inclusion of a few manganese oxides in the carbon for application to rechargeable Li–O_2 batteries. A dark-field TEM image (Fig. 8a)

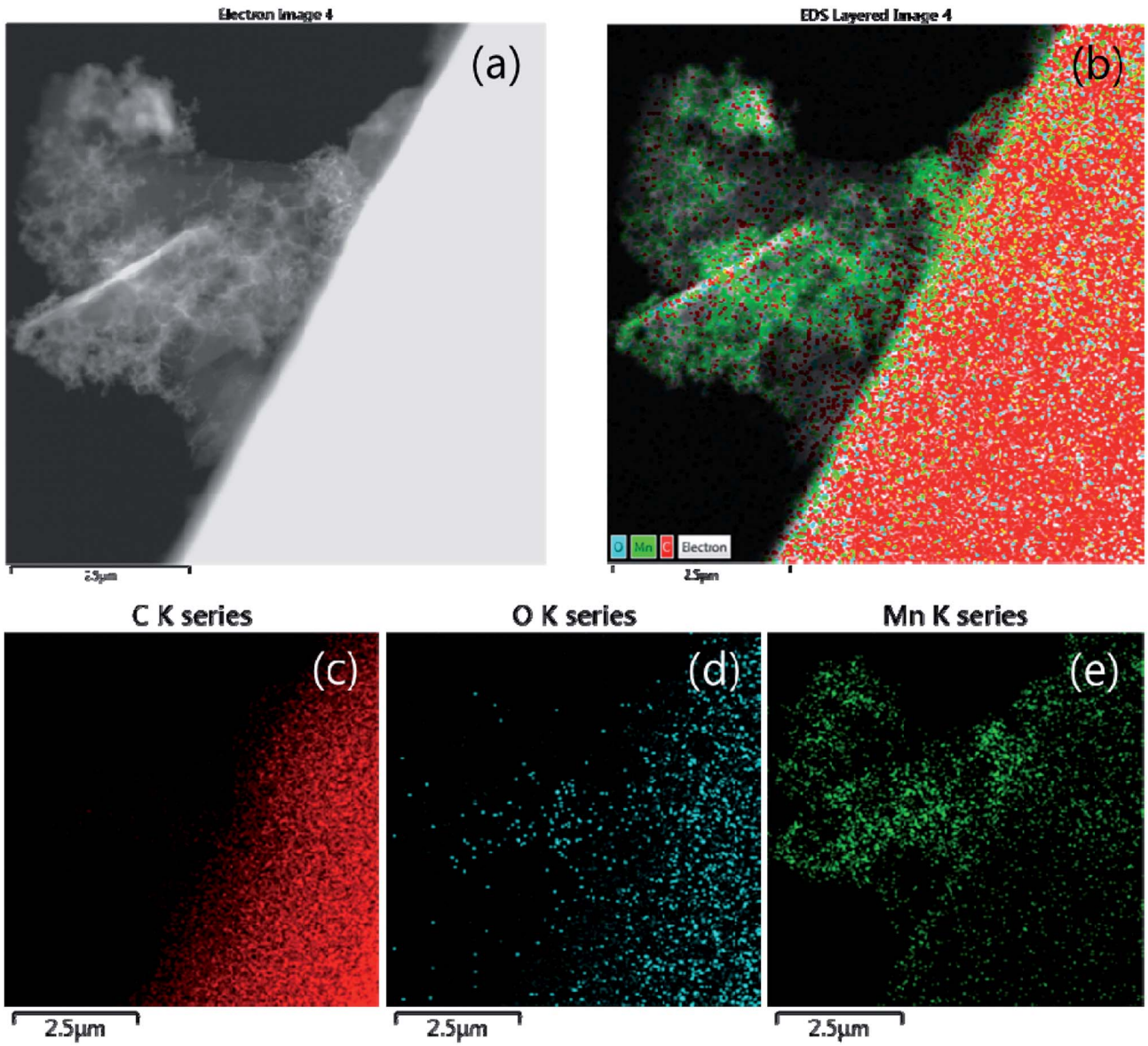

Fig. 8 (a) Dark field (b) elemental mapping images and corresponding elemental mapping images for (c) C, (d) O, and (e) Mn of partially oxidized Mn_3O_4-functionalized P50.

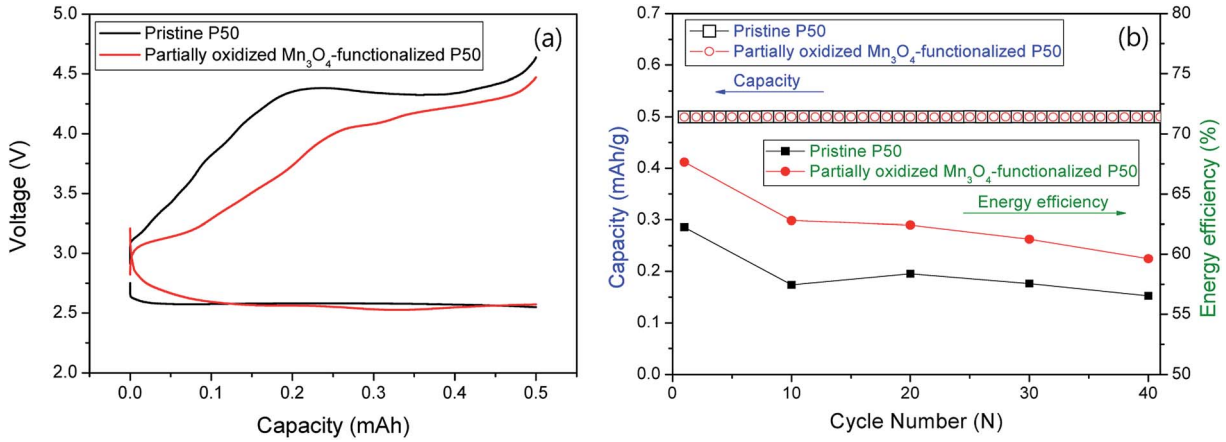

Fig. 9 (a) First discharge/charge graph and (b) cycle performances and energy efficiency for nonaqueous Li–O_2 cells.

also shows amorphous carbon on carbon nanofiber features, and this was confirmed by elemental mapping for C (Fig. 8c), O (Fig. 8d) and Mn (Fig. 8e), respectively. In pristine P50 (Fig. S2 in the ESI†), there are no manganese elements, however the Mn element is seen dispersed on the assignment of the dark field image (Fig. 8a), which is also shown in Fig. 8e. This evidence also demonstrates that manganese oxide is well-functionalized on the carbon surface.

Fig. 9 shows the electrochemical properties at a current of 0.1 mA for 5 h (limited capacity: 0.5 mA h); (a) first discharge/charge profiles and (b) cycle performances and energy efficiency for nonaqueous Li–O_2 cells. The pristine and partially oxidized Mn_3O_4-functionalized P50 cathodes in the Li–O_2 cells (Fig. 9a) show an average discharge potential of 2.6 V, which is similar to that determined in previous reports.[22–24] However, Fig. 9a shows a reduction in the charge overpotential: during charging, the energy efficiency of ~8% is increased in the cell where partially oxidized Mn_3O_4-functionalized P50 is applied to cathodes (red), compared to the pristine one (black). This increased energy efficiency is maintained during 40 cycles, although the degree decreases as the cycling proceeds, as shown in Fig. 9b.

Conclusion

In this study, partially oxidized Mn_3O_4-functionalized P50 was prepared by dipping carbon paper (P50) in Mn-acetate solution and heating at 300 °C to apply manganese oxide directly on the carbon. Results showed an improvement in the contact between carbon and the oxide, but only a small amount of the oxide species (<5%) showed catalytic effects during charge in a rechargeable Li–O_2 cell. This study proposes a simple synthetic route involving oxide application to the carbon surface. Results show that the reduced gravimetric capacity for heavy metal is relieved when using oxide catalysts in Li–O_2 cells.

Conflicts of interest

There are no conflicts to declare.

Acknowledgements

This Research was supported by Research Funds of Mokpo National University in 2017.

References

1 G. Girishkumar, B. McCloskey, A. C. Luntz, S. Swanson and W. Wilcke, *J. Phys. Chem. Lett.*, 2010, **1**, 2193.
2 M. Balaish, A. Kraytsberg and Y. Ein-Eli, *Phys. Chem. Chem. Phys.*, 2014, **16**, 2801.
3 P. G. Bruce, S. A. Freunberger, L. J. Hardwick and J.-M. Tarascon, *Nat. Mater.*, 2012, **11**, 19.
4 N.-S. Choi, Z. Chen, S. A. Freunberger, X. Ji, Y.-K. Sun, K. Amine, G. Yushin, L. F. Nazar, J. Cho and P. G. Bruce, *Angew. Chem., Int. Ed.*, 2012, **51**, 9994.
5 Y.-C. Lu, B. M. Gallant, D. G. Kwabi, J. R. Harding, R. R. Mitchell, M. S. Whittingham and Y. S. -Horn, *Energy Environ. Sci.*, 2013, **6**, 750–768.
6 A. C. Luntz and B. D. McCloskey, *Chem. Rev.*, 2014, **114**(23), 11721.
7 R. Black, B. Adams and L. F. Nazar, *Adv. Energy Mater.*, 2012, **2**, 801.
8 F. Li, T. Zhang and H. Zhou, *Energy Environ. Sci.*, 2013, **6**, 1125.
9 M. L. Thomas, K. Yamanaka, T. Ohta and H. R. Byon, *Chem. Commun.*, 2015, **51**, 3977.
10 Y. Chen, F. Li, D.-M. Tang, Z. Jian, C. Liu, D. Golberg, A. Yamada and H. Zhou, *J. Mater. Chem. A*, 2013, **1**, 13076.
11 Y.-C. Lu, H. A. Gasteiger, M. C. Parent, V. Chiloyan and Y. S. -Horn, *Electrochem. Solid-State Lett.*, 2010, **13**(6), A69–A72.
12 N. Ding, S. W. Chien, T. S. A. Hor, R. Lum, Y. Zong and Z. Liu, *J. Mater. Chem. A*, 2014, **2**, 12433.
13 J. S. Hummelshoj, J. Blomqvist, S. Datta, T. Vegge, J. Rossmeisl, K. S. Thygesen, A. C. Luntz, K. W. Jacobsen and J. K. Nørskov, *J. Chem. Phys.*, 2010, **132**, 071101.
14 Y. Shao, S. Park, J. Xiao, J.-G. Zhang, Y. Wang and J. Liu, *ACS Catal.*, 2012, **2**, 844.

15 R. Choi, J. Jung, G. Kim, K. Song, Y.-I. Kim, S. C. Jung, Y.-K. Han, H. Song and Y.-M. Kang, *Energy Environ. Sci.*, 2014, **7**, 1362.
16 E. Yilmaz, C. Yogi, K. Yamanaka, T. Ohta and H. R. Byong, *Nano Lett.*, 2013, **13**, 4679.
17 Z. Zhang, L. Su, M. Yang, M. Hu, J. Bao, J. Wei and Z. Zhou, *Chem. Commun.*, 2014, **50**, 776.
18 X. Zhang, C. Wang, Y.-N. Chen, X.-G. Wang, Z. Xie and Z. Zhou, *J. Power Sources*, 2018, **377**, 136.
19 X. Zhang, X. Zhang, X.-G. Wang, Z. Xie and Z. Zhou, *J. Mater. Chem. A*, 2016, **4**, 9390.
20 D. B. Radic, M. M. Stanojevi, M. O. Obradovic and A. M. Jovovic, *J. Therm. Sci.*, 2017, **21**, 1067.
21 E.-H. M. Diefallah, *Thermochim. Acta*, 1992, **202**, 1.
22 D. Sun, Y. Shen, W. Zhang, L. Yu, Z. Yi, W. Yin, D. Wang, Y. Huang, J. Wang, D. Wang and J. B. Goodenough, *J. Am. Chem. Soc.*, 2014, **136**, 8941.
23 E. N. Nasybulin, W. Xu, B. L. Mehdi, E. Thomsen, M. H. Engelhard, R. C. Masse, P. Bhattacharya, M. Gu, W. Bennett, Z. Nie, C. Wang, N. D. Browning and J.-G. Zhang, *ACS Appl. Mater. Interfaces*, 2014, **6**, 14141.
24 H. Nie, Y. Zhang, J. Li, W. Zhou, Q. Lai, T. Liu and H. Zhang, *RSC Adv.*, 2014, **4**, 17141.